A highly Crystalline Anthracene-based MOF-74 Series featuring Electrical Conductivity and Luminescence

Patricia I. Scheurle[‡†∇], Andre Mähringer[‡†∇], Andreas C. Jakowetz[†∇], Pouya Hosseini[∞], Alexander F. Richter[∇⊥], Gunther Wittstock[∞], Dana D. Medina[†∇*] and Thomas Bein[†∇*]

AUTHOR ADDRESSES

[†]Department of Chemistry, Ludwig-Maximilians-Universität (LMU), Butenandtstr. 5-13 (E), 81377 Munich, Germany.

[⊥]Chair for Photonics and Optoelectronics, Nano-Institute Munich, Department of Physics, Ludwig-Maximilians-Universität (LMU), Königinstr. 10, 80539 Munich, Germany.

[∇]Nanosystems Initiative Munich (NIM) and Center for NanoScience (CeNS), Schellingstr. 4, 80799 Munich, Germany.

[∞]Institute of Chemistry, Carl von Ossietzky Universität Oldenburg, 26111 Oldenburg, Germany.

ABSTRACT: Recently, a small group of metal-organic frameworks (MOFs) has been discovered featuring substantial charge transport properties and electrical conductivity, hence promising to broaden the scope of potential MOF applications in fields such as batteries, fuel cells and supercapacitors. In combination with light emission, electroactive MOFs are intriguing candidates for chemical sensing and optoelectronic applications. Here, we incorporated anthracene-based building blocks into the MOF-74 topology with five different divalent metal ions, that is, Zn^{2+}, Mg^{2+}, Ni^{2+}, Co^{2+} and Mn^{2+}, resulting in a series of highly crystalline MOFs, coined ANMOF-74(M). This series of MOFs features substantial photoluminescence, with ANMOF-74(Zn) emitting across the whole visible spectrum. The materials moreover combine this photoluminescence with high surface areas and electrical conductivity. Compared to the original MOF-74 materials constructed from 2,5-dihydroxy terephthalic acid and the same metal ions Zn^{2+}, Mg^{2+}, Ni^{2+}, Co^{2+} and Mn^{2+}, we observed a conductivity enhancement of up to six orders of magnitude. Our results point towards the importance of building block design and the careful choice of the embedded MOF topology for obtaining materials with desired properties such as photoluminescence and electrical conductivity.

Metal-organic frameworks (MOFs) are composed of metal ions or clusters that are interconnected by rigid organic building blocks forming crystalline porous structures.[1] Based on their well-defined and tunable pore spaces and high surface areas, many MOFs are attractive candidates for gas storage separation and storage applications.[2,3] Depending on the organic building blocks and the respective metal species, MOFs can be synthesized with diverse chemical composition, connectivity and functionality. Therefore, a large variety of different chemical and physical properties can be attained.[4,5,6] Recently, the intriguing property of electrical conductivity was added to this portfolio.[2,7–12] Hereby, an increasing number of MOFs were investigated with a view on applications in the fields of charge storage, semiconductors, chemical sensing, energy conversion or electrocatalysis.[12–20]

To date, only few MOFs have been reported exhibiting the desired property of electrical conductivity in combination with ultrahigh surface area, which is viewed to be essential for sensing or charge storage applications.[21] Recently, structures based on the MOF-74 topology constructed with 2,5-dihydroxy terephthalic acid were introduced as electrically conductive platforms.[2,5,22,23] MOF-74 isostructures connected through phenoxide-metal nodes showed low conductivity values, whereas structures containing sulfur ligating functionalities in the linking motif or mixed valance of the metal ions showed an increased electrical conductivity of up to 10^{-6} S cm^{-1}.[2,24]

Here, we present a series of MOF-74 analogs comprising an anthracene core in the linear organic linker. Anthracene and its derivatives are known for their high charge carrier mobility and electroluminescent properties.[11,21] We demonstrate that the incorporation of anthracene-containing building blocks can strongly enhance electrical conductivity in phenoxide-connected MOF-74 topologies. Furthermore, we show that the anthracene core endows the MOFs with photoluminescent properties allowing for the realization of light emitting and electrically conducting MOFs. For constructing the framework, we first established the synthesis of an anthracene-based building block modified with ortho-hydroxy para-carboxylic functionalities enabling the required bonding to metal ions, namely 4,4´-(anthracene-9,10-diyl)bis(2-hydroxybenzoic acid), ABHB.

Using the anthracene building blocks and divalent metal ions, that is, Zn^{2+}, Mg^{2+}, Ni^{2+}, Co^{2+} and Mn^{2+}, five novel, highly crystalline and porous anthracene-based MOF-74-type (ANMOF-74) materials were synthesis under solvothermal conditions (Figure 1). The ANMOF-74 series features an enhancement of electrical conductivity by several orders of magnitude compared to the respective original MOF-74 isostructures. Furthermore, the photoluminescence life time and quantum yield were determined for the ANMOF-74 series.
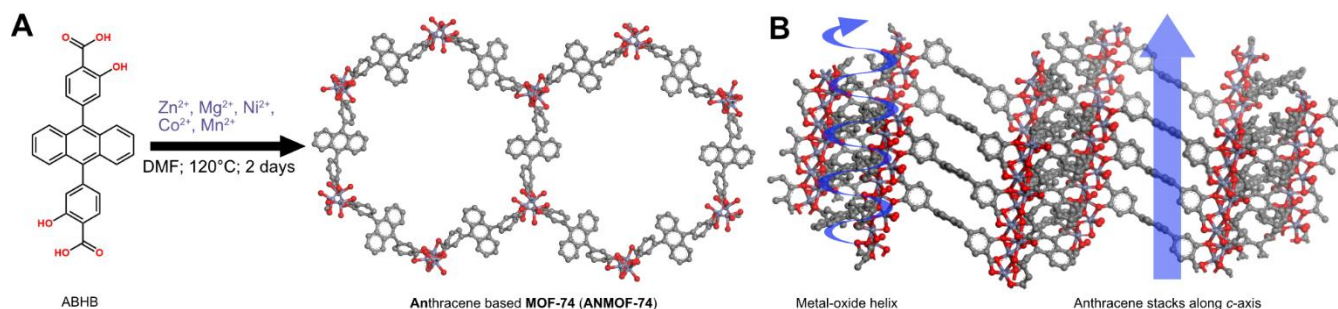

Figure 1. A) Synthesis scheme of the anthracene-based MOF-74 (ANMOF-74). The organic building block ABHB forms porous hexagonal frameworks with the respective metal ions. **B)** View on the helical metal-oxo chains of the ANMOF-74 structure *(left)* and the anthracene moieties *(right)* stacked along the crystallographic *c*-direction.

RESULTS AND DISCUSSION

The ABHB linker used here was synthesized *via* a three-step reaction procedure (see Schemes S1-S3).[25,26] In short, the reaction of methyl *4*-iodosalicylate and bis(pinacolato)diboron afforded a boronated intermediate product, which was subsequently coupled in a Suzuki reaction with the brominated anthracene core to the methyl protected ABHB linking motif. After deprotection and purification, the final organic building block ABHB was obtained in sufficient yields (ca. 70%) as a beige powder. For the MOF synthesis, the stoichiometric reaction of ABHB with the respective metal precursors (Zn^{2+}, Mg^{2+}, Ni^{2+}, Co^{2+} and Mn^{2+}) in different DMF/ MeOH/ EtOH/ BnOH/ H_2O mixtures at 120 °C for 2 days led to the precipitation of colored powders. Here, the color of the obtained powders was strongly dependent on the

3

utilized metal ion precursor (for further information see SI). The obtained powders were washed with DMF and methanol and subsequent dried under dynamic vacuum.
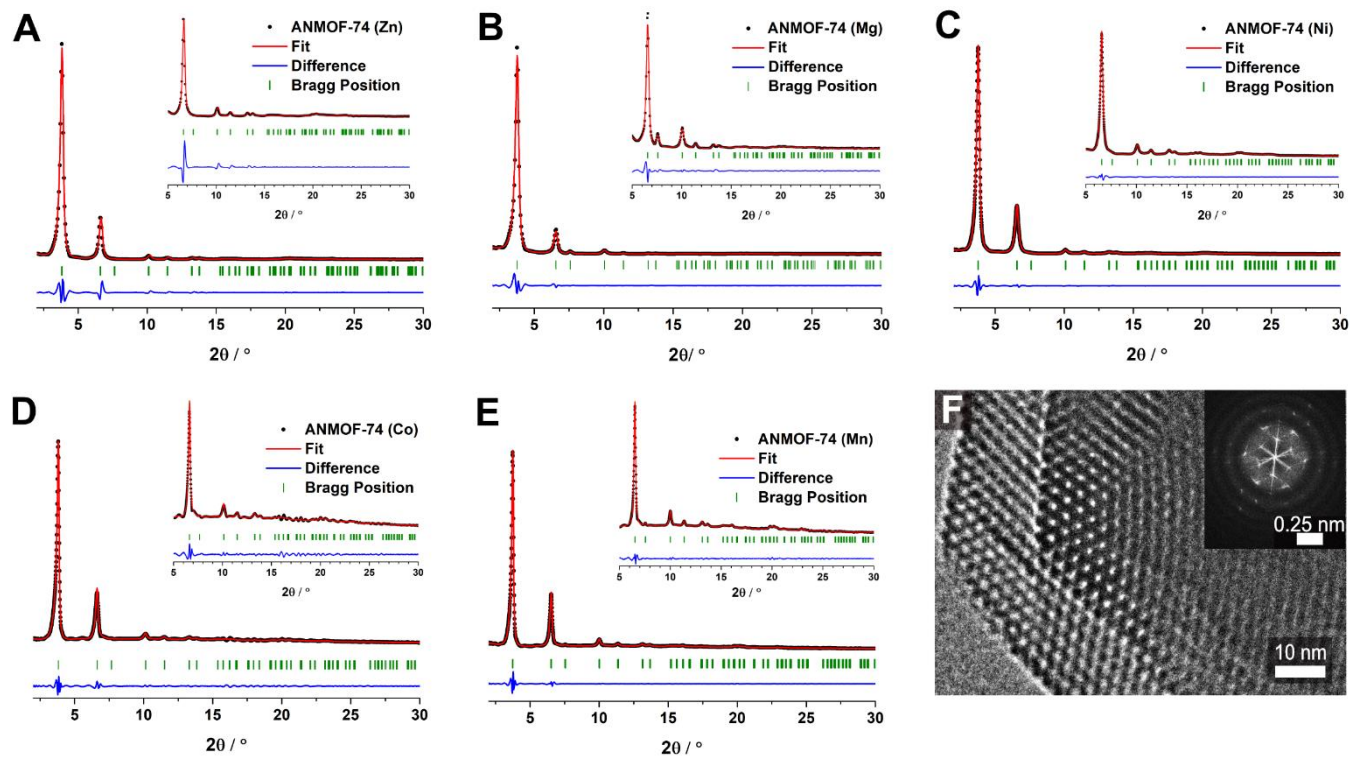

Figure 2. Experimental powder X-ray diffraction (PXRD) patterns of the ANMOF-74(M) series showing **(A)** the Zn-, **(B)** Mg-, **(C)** Ni-, **(D)** Co- and **(E)** Mn-MOF derivatives, respectively (black). The simulated PXRD pattern was Pawley-refined (red) according to the experimental data, whereby the difference plot is depicted in blue. The respective Bragg positions of the predicted hexagonal unit cell are shown as green bars. **(F)** A high resolution TEM image of an ANMOF-74 (Co) crystal oriented along the [001] axis with FFT of the entire image as inset.

Powder X-ray diffraction (PXRD) data of the dried powders are shown in Figure 2. All materials exhibit a high degree of crystallinity with pronounced reflections at 3.75°, 6.51°, 10.02°, 11.34°, 13.14° and 13.66° 2θ. Bragg reflections at up to 25° 2θ could be detected, underlining the high crystallinity of

the obtained ANMOF-74 series. The collected diffractograms matched with the ones predicted from simulated model structures. The predicted model structures were obtained with *Accelrys Materials Studio 7.0* using the calculated MOF-74 structure as a model.[2] After establishing the simulated unit cell, a PXRD pattern was calculated, which was Pawley-refined according to the respective experimental PXRD patterns (R_{wp} ranging from 2.09-4.09%). From the refinement, we conclude that the ANMOF-74 system crystallizes in the trigonal space group *R3* with $a = b = 46.3$ Å, c = 5.7 Å, $\alpha = \beta = 90°$ and $\gamma = 120°$. These findings are in good agreement with simulations performed for related MOF-74 structures.[11,27] All ANMOF-74 materials exhibit one-dimensional hexagonal channels with pore apertures of 2 nm. These channels are formed by the ABHB units that are interconnected in the *c*-direction by infinite helical metal-oxo chains. ANMOF-74 further includes infinite stacks of the anthracene core arranged along the *c*-direction, with the distance between adjacent anthracene cores estimated to be 5.7 Å (Figure 1B). For the ABHB unit, we determined a torsion angle of 60.7° between the benzene rings and the anthracene core. Transmission electron microscopy (TEM) analysis of the ANMOF-74 series revealed highly crystalline materials (Figure S2). For ANMOF-74(Co), hexagonally shaped crystal facets and large cross-section domain sizes of about 120 nm illustrate the high degree of crystallinity (Figure 2F). The calculated diffraction pattern in the fast Fourier transform (FFT) of the TEM image shows angles of 120° in accordance with the proposed trigonal crystal system.

The synthesized powders were further investigated using X-ray photoelectron spectroscopy (XPS). As summarized in Figures S12-S16, XPS spectra of ANMOF-74(M) show the presence of the respective metal, C and O peaks attributed to the MOFs, as well as nitrogen, tentatively attributed to DMF residues coordinating to the metal ions in the structure. These findings are in accordance with the high-resolution analysis of the O 1s regions in the XPS spectra of all ANMOFs, indicating three types of oxygen atoms. The signals can be assigned to the functional groups (carboxy and hydroxy) of the ligating building block and to the oxygen related to DMF. Only ANMOF-74(Zn) has a second N 1s peak arising from residual NO_3^-, which apparently originates from the $Zn(NO_3)_2$ synthesis precursor. Importantly, Cl^- or

additional N peaks related to impurities originating from the metal precursors were not observed for all other samples of the ANMOF-74 series. The purity of the obtained materials was further studied by energy dispersive X-ray spectroscopy (EDX) which showed no impurities arising from precursor anions (see Figure S11). Thermogravimetric analysis (TGA) revealed that the ANMOF-74(M) materials were not decomposed below 300 °C under dynamic conditions (Figure S10).
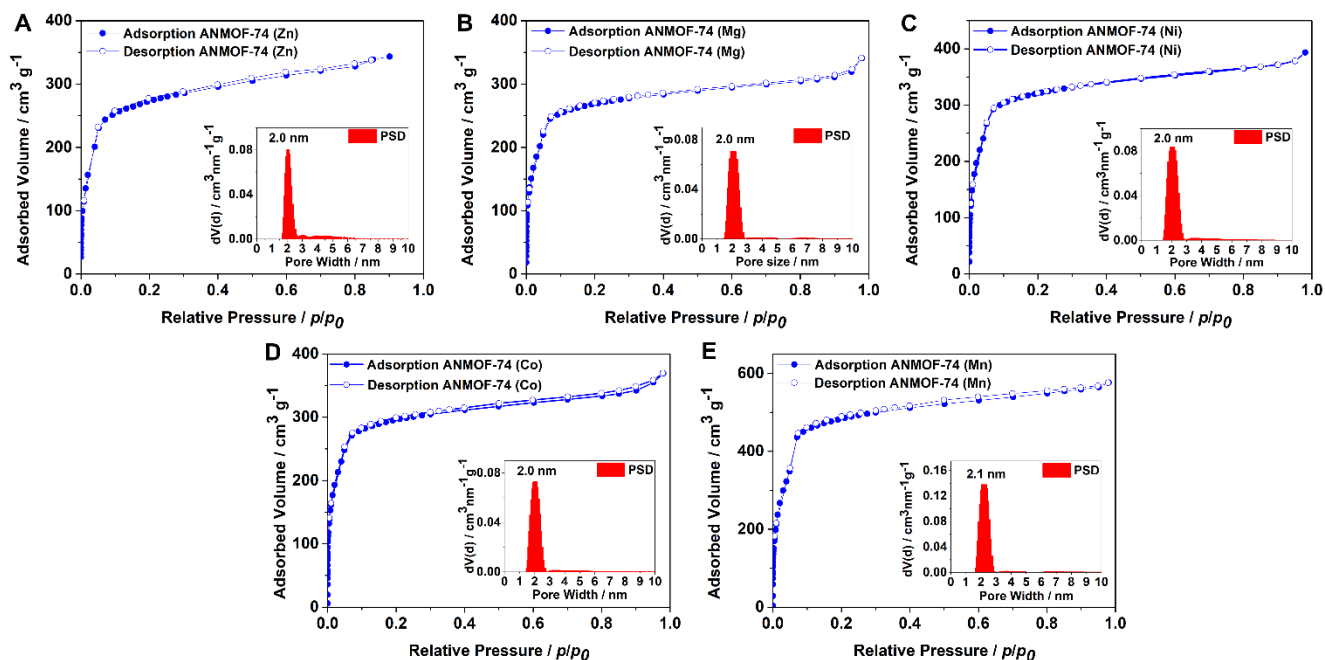

Figure 3. Nitrogen physisorption isotherms of (**A**) ANMOF-74(Zn), (**B**) ANMOF-74(Mg), (**C**) ANMOF-74(Ni), (**D**) ANMOF-74(Co) and (**E**) ANMOF-74(Mn) showing *Type I(b)* shape. The ad- and desorption branches are depicted as blue and white colored circles, respectively. Pore size distributions (PSD) are included as insets.

The pore accessibility of the activated samples was investigated by nitrogen physisorption experiments. The nitrogen isotherms (77 K) of all ANMOF-74(M) powders (Figure 3) show IUPAC *Type I(b)*[28] sorption behavior, indicating that the ANMOF-74(M) form large micropores (< 2.5 nm). All examined MOFs show an initial uptake of about 200 cm^3g^{-1} at low pressures and a second uptake at 0.02-0.05 *p/p₀* of about 100 cm^3g^{-1}. The adsorption branch and the desorption branch merge at low relative pressures

6

illustrating a reversible process. The Brunauer-Emmett-Teller (BET) surface areas and total pore volumes for the ANMOF-74(M) bulk materials series were calculated to be 1124 $m^2 g^{-1}$ and 0.49 $cm^3 g^{-1}$ for Zn, 1137 $m^2 g^{-1}$ and 0.48 $cm^3 g^{-1}$ for Mg, 1352 $m^2 g^{-1}$ and 0.56 $cm^3 g^{-1}$ for Ni, 1213 $m^2 g^{-1}$ and 0.53 $cm^3 g^{-1}$ for Co, 1748 $m^2 g^{-1}$ and 0.83 $cm^3 g^{-1}$ for Mn, respectively. The pore size distributions were calculated using quenched solid density functional theory (QSDFT), giving pore sizes of 2.1 nm in ANMOF-74(Mn) and 2.0 nm in all other ANMOF-74(M) structures, which match the predicted value of 2.0 nm obtained by the simulated structure. Connolly surface area calculations with nitrogen as a probe molecule (2.6 Å) predict a theoretical surface area of 1757 $m^2 g^{-1}$, which is matched best by the BET results for the ANMOF-74(Mn) sample.

Scanning electron microscopy (SEM) images of the ANMOF-74(M) powders reveal needle-shaped crystallites forming spherical agglomerates (Figures 4 and S2). In addition, high magnification SEM analysis reveals crystallites with a well-faceted hexagonal cross-section, further confirming the proposed trigonal crystal structures.
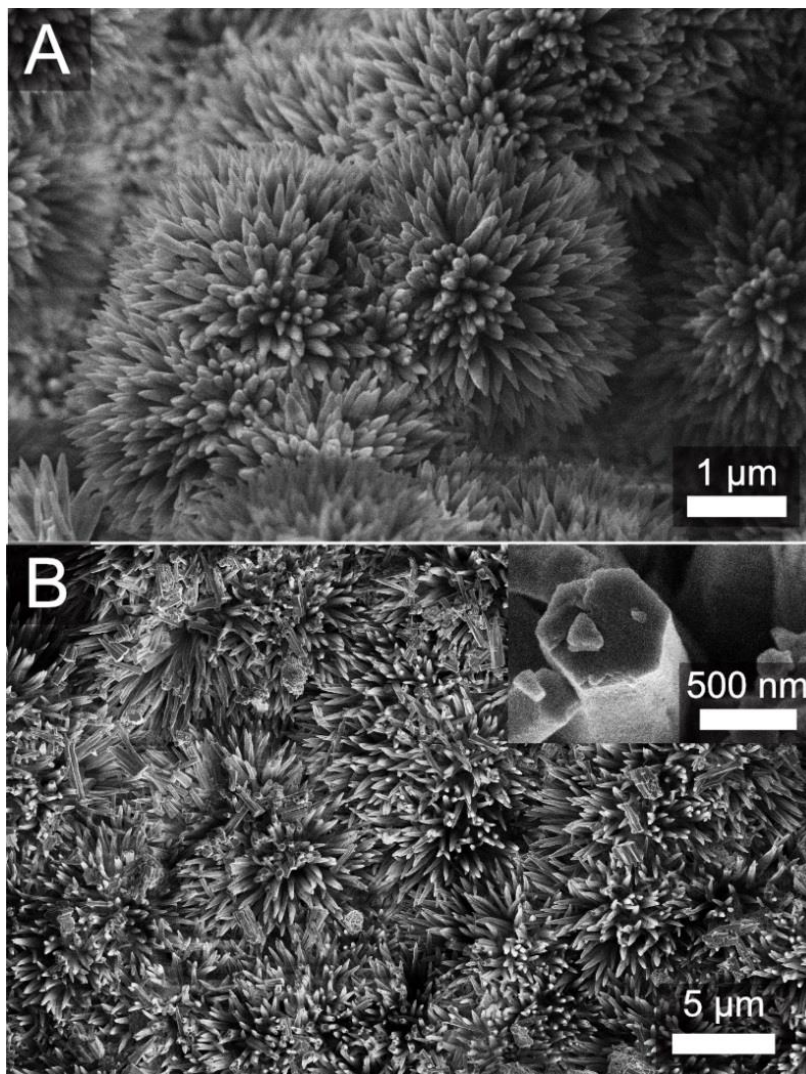
Figure 4. (**A**) and (**B**) SEM images of the ANMOF-74 bulk materials (**A**) ANMOF-74(Ni) (**B**) ANMOF-74(Mn) with a high magnification of a hexagonally shaped crystal depicted as inset.

To elucidate the electrical properties of the ANMOF-74 series, we performed four-point probe van der Pauw measurements of crystalline and pelleted samples (for further details see SI). The obtained results are summarized in Table 1.

Table 1. Electrical conductivity values of ANMOF-74(M) and MOF-74(M) samples obtained with pellets by using the four-probe van der Pauw technique.

ANMOF-74 (Zn)	MOF-74 (Zn)	ANMOF-74 (Mg)	MOF-74 (Mg)	ANMOF-74 (Ni)	MOF-74 (Ni)
6×10^{-8} S cm^{-1}	6×10^{-12} S cm^{-1}	5×10^{-9} S cm^{-1}	6×10^{-13} S cm^{-1}	4×10^{-7} S cm^{-1}	6×10^{-13} S cm^{-1}
ANMOF-74 (Co)	**MOF-74 (Co)**	**ANMOF-74 (Mn)**	**MOF-74 (Mn)**		
4×10^{-8} S cm^{-1}	6×10^{-13} S cm^{-1}	3×10^{-8} S cm^{-1}	4×10^{-13} S cm^{-1}		

The values obtained for ANMOF-74(M) range from 10^{-7} to 10^{-9} S cm^{-1}, corresponding to a striking increase of up to six orders of magnitude with regard to the values obtained (and reported) for the respective MOF-74. To validate the impact of the anthracene core on the electrical conductivity, crystalline MOF-74 powders with the same set of metal ions were synthesized, activated (vacuum dried), compressed into pellets and their electrical conductivity was evaluated. The van der Pauw measurements of the MOF-74 pellets confirmed the ANMOF-74 series to be substantially more conductive than the MOF-74 isostructures. We attribute the enhanced electrical conductivity to the presence of the electron-rich anthracene core incorporated in the ANMOF-74, in contrast to the rather electron-poor 2,5-dihydroxy terephthalic acid building block embedded in the MOF-74 series. Here, our strategy of embedding the electron-rich anthracene-based linker showed a remarkable increase in conductivity, however, the measured values are still modest compared to other conducting MOF platforms.[29,30] Due to the fairly large stacking distance between adjacent anthracene units we postulate that charge transport still occurs mostly through the metal-oxo backbone by charge carrier hopping between metal nodes.

To further elucidate the impact of the MOF-embedded anthracene moiety, we examined the optical properties of the ANMOF-74(M) bulk materials by using UV-vis absorption and photoluminescence (PL) spectroscopy, summarized in Figure 5. The UV-vis spectra were measured in diffusive reflectance geom-

etry and transformed using the Kubelka-Munk equation. For all examined ANMOF-74 samples the absorption bands are located in the UV and blue spectral regions. ANMOF-74(Zn) has an absorption onset of around 528 nm and a second one at around 450 nm, and ANMOF-74(Mg; Ni; Co; Mn) at around 440 nm. Tauc plots were analyzed, assuming direct band gaps, yielding an optical band gap of 2.86 eV for ANMOF-74(Zn) and in case of ANMOF-74(Mg; Ni; Co; Mn) band gaps between 2.91 eV and 2.95 eV (Figure S5). These five MOFs have two sharp absorption maxima at 400 nm and 380 nm, which originate from the integrated ABHB building blocks (see Figure S4 (A)).

Photoluminescence (PL) of the ANMOF-74(M) bulk materials was measured with a pulsed 378 nm excitation under argon atmosphere to protect the anthracene from degradation. The PL spectrum of ANMOF-74(Zn) shows a very broad emission band over the whole visible spectrum with a maximum at 570 nm and a large Stokes shift of 170 nm. ANMOF-74(Mg) and ANMOF-74(Co), as well as ANMOF-74(Ni) and ANMOF-74(Mn) have a narrow emission band with a small shoulder and an emission maximum between 438 nm and 444 nm, respectively. It is similar to the emission band at 441 nm of the ABHB linker monomer measured in solution (see Figure S4 (B)). These MOFs exhibit smaller Stokes shifts of 38 – 44 nm. ANMOF-74(Co) and ANMOF-74(Ni) also have a weaker emission band at 692 nm. ANMOF-74(Mn) has a weak emission band at 701 nm.
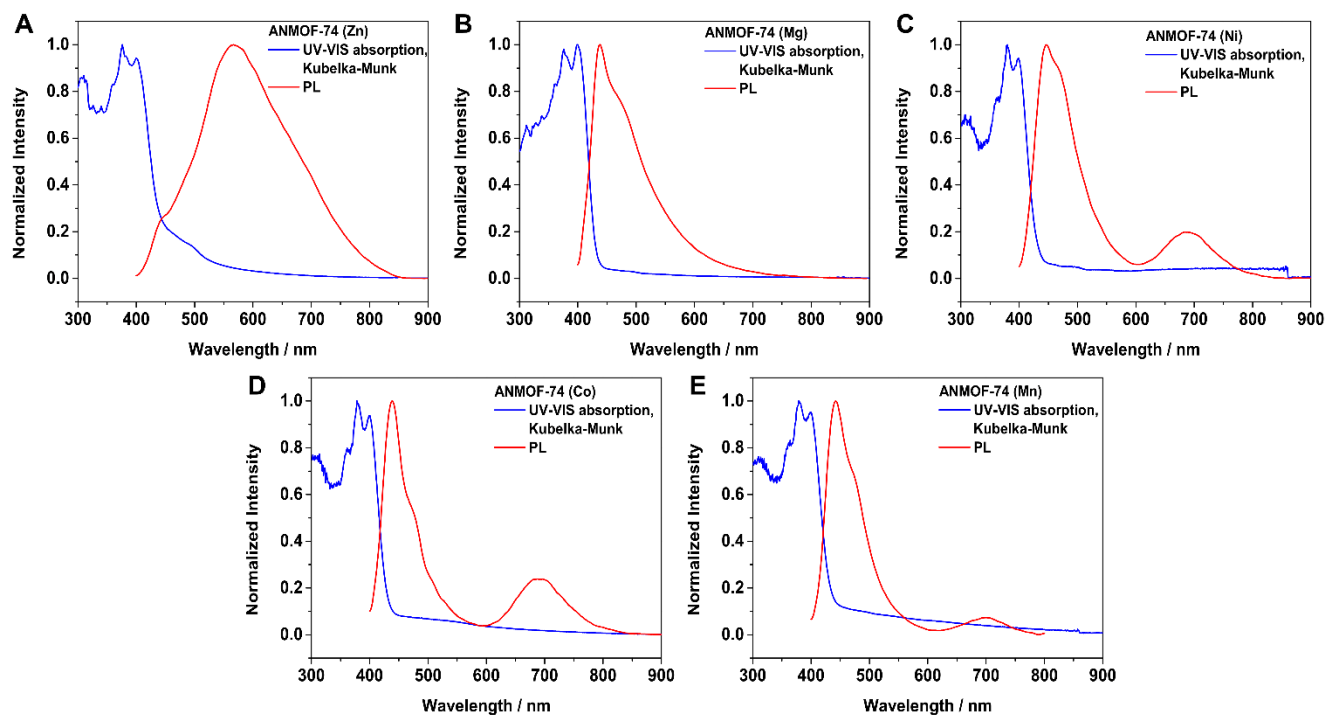
Figure 5. UV-VIS absorption measured in diffusive reflectance of the MOF powders dispersed with BaSO$_4$ (blue line) and the photoluminescence (PL) spectra of the neat MOF bulk materials measured with pulsed 378 nm excitation (red line): **A)** ANMOF-74(Zn), **B)** ANMOF-74(Mg), **C)** ANMOF-7(Ni), **D)** ANMOF-74(Co) and **E)** ANMOF-74(Mn).

Time-correlated single photon counting (TCSPC) traces of ANMOF-7(Zn) and ANMOF-74(Mg) were recorded at the respective emission maxima of 570 nm and 438 nm, shown in Figure 6. Both MOFs show very similar relaxation behavior, analyzed with a triexponential fit. Both exhibit fast decays of around $\tau_1 = 0.16$ ns, which is near the instrumental response limit. The medium component has a lifetime τ_2 of 0.79 ns and 1.03 ns while the third component has a lifetime τ_3 of 3.44 ns and 4.90 ns for Zn and Mg, respectively. The main difference between the two materials is the fractional distribution of lifetimes. While the medium-lifetime decay channel is contributing almost 60% to the overall emission in the ANMOF-74(Zn) and only 50% in the ANMOF-74(Mg), this difference is balanced by the longer lifetime components, i.e. 18% versus 29% in the Zn and Mg ANMOFs, respectively. This results in the faster

11

overall decay of the ANMOF-74(Zn) as compared to the longer-lived ANMOF-7(Mg). Due to the bright emission and long lifetime of ANMOF-74(Mg), we also measured the photoluminescence quantum yield (PLQY), which reaches 2.5%. Quantum efficiency of the ABHB linker molecules as solid powder show PLQY values of up to 13%, which is reduced by one order of magnitude upon incorporation into the framework. However, the luminescence is still detectable with the naked eye by irradiating the Mg-ANMOF sample with a UV lamp.

TCSPC traces of ANMOF-74(Ni), ANMOF-74(Co) and ANMOG-74(Mn) show similar lifetime components with τ_1 around 0.06 ns, τ_2 between 0.79 ns and 0.89 ns and τ_3 in the range of $5 - 7$ ns (see Figure S6). The ABHB linker monomer has a monoexponential decay with a lifetime of 4.3 ns (see S6). The long PL lifetime of ANMOF-74(Mg) in comparison to the other ANMOFs might be related to the different emission spectrum. ANMOF-74(Mg), similar to the ABHB linker, does not have a second emission band at around 700 nm. But the PL lifetime of ANMOF-74(Mg) and of the ABHB linker are much longer compared to the other ANMOFs. Thus, in the ANMOF-74(Mg), the linkers might be similarly electronically ´isolated` as the monomer in solution while the emission band at around 700 nm might be related to electronic interactions between linkers (and transition metal ions), effectively decreasing the PL lifetime.
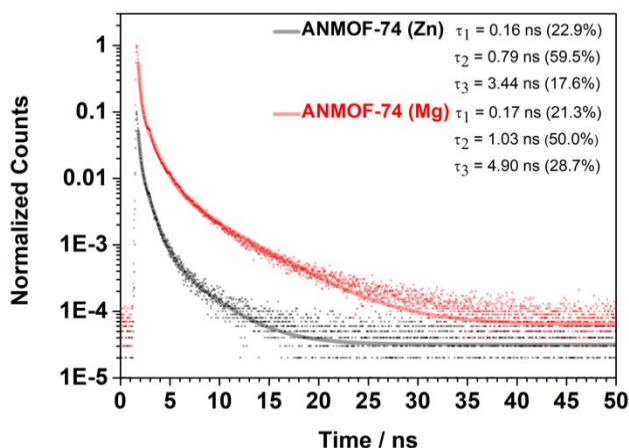
Figure 6. The time-correlated single photon counting (TCSPC) traces corresponding to the PL spectra of ANMOF-74(Zn) (black) and ANMOF-74(Mg) (red), which were recorded at the respective emission maximum of each MOF. The lifetimes were obtained from triexponential fits (solid lines) to the data (scatter). The fractions of emitted photons corresponding to the respective lifetimes are stated in brackets.

CONCLUSIONS

In our study, we present the successful synthesis of a novel series of metalorganic frameworks showing MOF-74 topology, coined ANMOF-74. The frameworks are built from anthracene-based linking motifs (ABHB) connected *via* helical metal-oxo chains, whereby a range of different metal ions could be incorporated (Zn, Mg, Co, Ni and Mn) into the framework. All ANMOF-74 materials feature a high degree of crystallinity and show BET surface areas exceeding 1000 m^2g^{-1}. Furthermore, all ANMOF-74 materials exhibit an enhancement of electrical conductivity of up to one-million fold compared to regular MOF-74. The ANMOF-74 materials feature direct optical band gaps of around 2.9 eV and most show photoluminescence in the blue spectral region. In contrast to the other derivatives, the ANMOF-74(Mg) shows a rather high quantum efficiency of 2.5%. Remarkably, ANMOF-74(Zn) emits photoluminescence

across the entire visible spectrum. We believe that this promising combination of high crystallinity, defined porosity, luminescence as well as electrical conductivity embedded in a fixed MOF matrix will enable a range of possible applications such as sensing and charge storage. Our study highlights the great versatility of the MOF-74 topology, allowing for the integration of sterically demanding organic linker structures with interesting electrical and optical properties. In the future, we envision the integration of additional chromophores with interesting optoelectronic properties and a tunable degree of electronic coupling into this highly attractive MOF topology, to further broaden the field of MOF-74 based structures for optoelectronic applications.

ASSOCIATED CONTENT

Supporting Information

Supporting Information is provided for the experimental details of the characterization techniques, the synthesis of all compounds and preparation of the samples and characterization using SEM, TEM, UV-vis absorption, PL, TGA, EDX and XPS.

AUTHOR INFORMATION

Corresponding Author

*Email: bein@lmu.de
*Email: dana.medina@cup.uni-muenchen.de

Present Addresses

†If an author's address is different than the one given in the affiliation line, this information may be included here.

Author Contributions

‡ P. S. and A. M. contributed equally. The manuscript was written through contributions of all authors. All authors commented on the manuscript.

ABBREVIATIONS

ANMOF-74, anthracene-based metal-organic framework-74; BET, Brunauer-Emmett-Teller; BnOH, benzyl alcohol; DMF, diemthylformamide; EtOH, ethanol; FFT, fast Fourier transform; PXRD, powder X-ray diffraction; SEM, scanning electron microscopy; MeOH, methanol; TEM, transmission electron microscopy; SBU, secondary building unit, PL, photoluminescence, PLQY, photoluminescence quantum yield; TCSPC, time-correlated single photon counting; TGA, thermogravimetric analysis; UV-VIS spectroscopy, ultraviolet-visible spectroscopy; PSD, pore size distribution; XPS, X-ray photoelectron spectroscopy.

References

(1) Yaghi, O. M.; Li, H. Hydrothermal Synthesis of a Metal-Organic Framework Containing Large Rectangular Channels. *J. Am. Chem. Soc.* **1995**, 10401–10402.

(2) Sun, L.; Hendon, C. H.; Minier, M. A.; Walsh, A.; Dincă, M. Million-Fold Electrical Conductivity Enhancement in Fe2(DEBDC) versus Mn2(DEBDC) (E = S, O). *J. Am. Chem. Soc.* **2015**, *137*, 6164–6167.

(3) Meek, S. T.; Greathouse, J. A.; Allendorf, M. D. Metal-Organic Frameworks: A Rapidly Growing Class of Versatile Nanoporous Materials. *Adv. Mater.* **2011**, *23*, 249–267.

(4) Wang, L. J.; Deng, H.; Furukawa, H.; Gándara, F.; Cordova, K. E.; Peri, D.; Yaghi, O. M. Synthesis and Characterization of Metal-Organic Framework-74 Containing 2, 4, 6, 8, and 10 Different Metals. *Inorg. Chem.* **2014**, *53*, 5881–5883.

(5) Kapelewski, M. T.; Geier, S. J.; Hudson, M. R.; Stück, D.; Mason, J. A.; Nelson, J. N.; Xiao, D. J.; Hulvey, Z.; Gilmour, E.; FitzGerald, S. A. *et al.* M2(m-dobdc) (M = Mg, Mn, Fe, Co, Ni) metal-organic frameworks exhibiting increased charge density and enhanced H2 binding at the open metal sites. *J. Am. Chem. Soc.* **2014**, *136*, 12119–12129.

(6) Rosi, N. L.; Kim, J.; Eddaoudi, M.; Chen, B.; O'Keeffe, M.; Yaghi, O. M. Rod packings and metal-organic frameworks constructed from rod-shaped secondary building units. *J. Am. Chem. Soc.* **2005**, *127*, 1504–1518.

(7) Usman, M.; Mendiratta, S.; Batjargal, S.; H., G.; Haider, M.; Rao Gade, N.; Chen, J.-W.; Chen, Y.-F.; Lu, K.-L. Semiconductor Behavior of a Three-Dimensional Strontium-Based Metal-Organic Framework. *ACS Appl. Mater. Interfaces* **2015**, *7*, 22767–22774.

(8) Sun, L.; Campbell, M. G.; Dincă, M. Electrically Conductive Porous Metal-Organic Frameworks. *Angew. Chem.* **2016**, *55*, 3566–3579.

(9) Usman, M.; Mendiratta, S.; Lu, K.-L. Semiconductor Metal-Organic Frameworks: Future Low-Bandgap Materials. *Adv. Mater.* **2017**, *29*, 1605071.

(10) Kobayashi, Y.; Jacobs, B.; Allendorf, M. D.; Long, J. R. Conductivity, Doping, and Redox Chemistry of a Microporous Dithiolene-Based Metal−Organic Framework. *Chem. Mater.* **2010**, *22*, 4120–4122.

(11) Guo, Z.; Panda, D. K.; Gordillo, M. A.; Khatun, A.; Wu, H.; Zhou, W.; Saha, S. Lowering Band Gap of an Electroactive Metal-Organic Framework via Complementary Guest Intercalation. *ACS Appl. Mater. Interfaces* **2017**, *9*, 32413–32417.

(12) Stavila, V.; Talin, A. A.; Allendorf, M. D. MOF-based electronic and opto-electronic devices. *Chem. Soc. Rev.* **2014**, *43*, 5994–6010.

(13) Campbell, M. G.; Sheberla, D.; Liu, S. F.; Swager, T. M.; Dincă, M. Cu₃(hexaiminotriphenylene)₂: an electrically conductive 2D metal-organic framework for chemiresistive sensing. *Angew. Chem.* **2015**, *54*, 4349–4352.

(14) Zhang, Z.; Yoshikawa, H.i.; Awaga, K. Monitoring the solid-state electrochemistry of Cu(2,7-AQDC) (AQDC = anthraquinone dicarboxylate) in a lithium battery: coexistence of metal and ligand redox activities in a metal-organic framework. *J. Am. Chem. Soc.* **2014**, *136*, 16112–16115.

(15) Campbell, M. G.; Dincă, M. Metal-Organic Frameworks as Active Materials in Electronic Sensor Devices. *Sensors* **2017**, *17*, 1106.

(16) Kreno, L. E.; Leong, K.; Farha, O. K.; Allendorf, M.; van Duyne, R. P.; Hupp, J. T. Metal-organic framework materials as chemical sensors. *Chem. Rev.* **2012**, *112*, 1105–1125.

(17) Zhu, X.-D.; Zhang, K.; Wang, Y.; Long, W.-W.; Sa, R.-J.; Liu, T.-F.; Lü, J. Fluorescent Metal-Organic Framework (MOF) as a Highly Sensitive and Quickly Responsive Chemical Sensor for the Detection of Antibiotics in Simulated Wastewater. *Inorg. Chem.* **2018**, *57*, 1060–1065.

(18) Yi, F.-Y.; Chen, D.; Wu, M.-K.; Han, L.; Jiang, H.-L. Chemical Sensors Based on Metal-Organic Frameworks. *ChemPlusChem* **2016**, *81*, 675–690.

(19) Kim, H.; Rao, S. R.; Kapustin, E. A.; Zhao, L.; Yang, S.; Yaghi, O. M.; Wang, E. N. Adsorption-based atmospheric water harvesting device for arid climates. *Nat. Commun.* **2018**, *9*, 1191.

(20) Gérard, F.; Millange, F.; Morcrette, M.; Serre, C.; Doublet, M.-L.; Grenèche, J.-M.; Tarascon, J.-M. Mixed-valence li/fe-based metal-organic frameworks with both reversible redox and sorption properties. *Angew. Chem.* **2007**, *46*, 3259–3263.

(21) Chen, D.; Xing, H.; Su, Z.; Wang, C. Electrical conductivity and electroluminescence of a new anthracene-based metal-organic framework with π-conjugated zigzag chains. *Chem. Commun.* **2016**, *52*, 2019–2022.

(22) Deng, H.; Grunder, S.; Cordova, K. E.; Valente, C.; Furukawa, H.; Hmadeh, M.; Gándara, F.; Whalley, A. C.; Liu, Z.; Asahina, S. *et al.* Large-pore apertures in a series of metal-organic frameworks. *Science* **2012**, *336*, 1018–1023.

(23) Cozzolino, A. F.; Brozek, C. K.; Palmer, R. D.; Yano, J.; Li, M.; Dincă, M. Ligand redox non-innocence in the stoichiometric oxidation of Mn2(2,5-dioxidoterephthalate) (Mn-MOF-74). *J. Am. Chem. Soc.* **2014**, *136*, 3334–3337.

(24) Sun, L.; Miyakai, T.; Seki, S.; Dincă, M. Mn2(2,5-disulfhydrylbenzene-1,4-dicarboxylate): a microporous metal-organic framework with infinite (-Mn-S-)∞ chains and high intrinsic charge mobility. *J. Am. Chem. Soc.* **2013**, *135*, 8185–8188.

(25) Fracaroli, A. M.; Furukawa, H.; Suzuki, M.; Dodd, M.; Okajima, S.; Gándara, F.; Reimer, J. A.; Yaghi, O. M. Metal-organic frameworks with precisely designed interior for carbon dioxide capture in the presence of water. *J. Am. Chem. Soc.* **2014**, *136*, 8863–8866.

(26) Hirofumi, M.; Akira, S.; Yusuke, M.; Yoshinori, I. Polycarboxylic acid containing condensed aromatic ring, crystalline network complex using same, and gas storage material. *WO 2017006638 A1* **2017**.

(27) Zheng, J.; Vemuri, R. S.; Estevez, L.; Koech, P. K.; Varga, T.; Camaioni, D. M.; Blake, T. A.; McGrail, B. P.; Motkuri, R. K. Pore-Engineered Metal-Organic Frameworks with Excellent Adsorption of Water and Fluorocarbon Refrigerant for Cooling Applications. *J. Am. Chem. Soc.* **2017**, *139*, 10601–10604.

(28) Thommes, M.; Kaneko, K.; Neimar K, A. V.; Olivier, J. P.; Rodriguez-Reinoso, F.; Rouquerol, J.; Sing, K. S. W. Physisorption of gases, with special reference to the evaluation of surface area and pore size distribution (IUPAC Technical Report). *Pure Appl. Chem.* **2015**, *87*, 1051–1069.

(29) Ko, M.; Mendecki, L.; Mirica, K. Conductive two-dimensional metal-organic frameworks as multifunctional materials. *Chem. Commun.* **2018**, *54*, 7873–7891.

(30) Mähringer, A.; Jakowetz, A. C.; Rotter, J. M.; Bohn, B. J.; Feldmann, J.; Bein, T.; Medina, D.D. oriented Thin Films of Electroactive Triphenylene catecholate-Based 2D Metal-Organic Frameworks. *ACS Nano,* **2019**.